SAND2022-xxxxR, R&A Tracking number 1641019.

LDRD Project Number: 228239

LDRD PROJECT TITLE: Internal 2-D Surface Temperature Measurements for Large Complex Geometries

PROJECT TEAM MEMBERS: Magnus Sjöberg, Nathan Prisbrey, and Wyatt Hodges

ABSTRACT:

For 2D-temperature monitoring applications, a variant of EIT (Electrical Impedance Tomography) is evaluated computationally in this work. Literature examples of poor sensor performance in the center of the 2D domains away from the side electrodes motivated this study which seeks to overcome some of the previously noted shortcomings. In particular, the use of 'sensing skins' with novel tailored baseline conductivities were examined using the EIDORS package for EIT. It was found that the best approach for detecting a hot spot depends on several factors such as the current injection (stimulation) patterns, the measurement patterns, and the reconstruction algorithms. For a well-performing combination of these factors, tailored baseline conductivities were assessed and compared to the baseline uniform conductivity. It was discovered that for some EIT applications, a tailored distribution needs to be smooth and that sudden changes in the conductivity gradients should be avoided. Still, the benefits in terms of improved EIT performance were small for conditions for which the EIT measurements had been 'optimized' for the uniform baseline case. Within the limited scope of this study, only two specific cases showed benefits from tailored distributions. For one case, a smooth tailored distribution with increased baseline conductivity in the center provided a better separation of two centrally located hot spots. For another case, a smooth tailored distribution with reduced conductivity in the center provided better estimates of the magnitudes of two hot spots near the center of the sensing skin.

INTRODUCTION AND EXECUTIVE SUMMARY OF RESULTS:

Across various industrial disciplines, there are numerous applications which have a strong need to monitor internal temperatures of large machineries and assemblies, sometimes with complex (*i.e.*, not flat) internal structures. As a particular example, battery-based grid storage solutions are very expensive, and any battery cell failure must be detected early so that a catastrophic cascading thermal-runaway situation can be avoided [1]. Brute-force installation of thermocouples to monitor 2D-temperature fields in spaces between large battery packs, however, may lead to an excessive amount of wiring. For example, if a 2 cm spatial resolution is required for a square surface of 1 m x 1 m, approximately 2500 thermocouples would be required, with an

associated 5000 individual wires. If the same 1 m^2 area could be monitored with electrodes attached along the four edges, only 200 wires would be required if the same 2 cm spacing is applied. With this motivation, a variant of EIT (Electrical Impedance Tomography) is considered in this work, sometimes called Electrical Resistance tomography (ERT) [2]. The detection principle uses a 'temperature sensing skin', for which the local electrical conductivity goes down with a local increase of temperature (*i.e.*, a hot spot). This change is detected indirectly by monitoring the changes in voltage potential at discrete locations (*i.e.,* electrodes) along the edges of the 2D surface being monitored, with the voltage being a result of current injection into the electrodes following predetermined stimulation patterns. While the results of Rashetnia *et al.* [2] indicated potential of this 2D temperature monitoring application of EIT, the publication included examples of poor sensor performance in the center of the 2D domain. Said performance motivated this study, which seeks to overcome some of the previously noted shortcomings. In particular, the use of novel 'sensing skins' with tailored baseline conductivities are examined here.

This work was performed computationally using the EIDORS package for EIT, executed in MATLAB. It was found that the best approach for detecting a hot spot depends on several factors. In particular, the magnitude of the relative reduction in local conductivity matters greatly, suggesting that EIT is most promising for combinations of large temperature changes and sensing skins with high temperature coefficient of resistance. Additionally, three factors have a great influence on the result: the current injection (stimulation) patterns, the measurement patterns, and the reconstruction algorithms. For a well-performing combination of these factors, tailored baseline conductivities were assessed and compared to the baseline uniform conductivity. The study covered many combinations of the factors above with various hot-spot distributions and baseline conductivity distributions. It was discovered that for some EIT conditions reconstruction artifacts can occur if the tailored conductivity distribution has sudden changes in the conductivity gradients. Hence, sudden changes in the conductivity gradients should be avoided by the use of smooth distributions with gradually changing conductivity gradients. Two different smooth distributions were assessed: one with higher baseline conductivity near the center of the measurement domain, and another with reduced baseline conductivity near the center. Simulations confirmed that the changes to the conductivity distribution had a substantial influence on the voltage distribution and the current-flow patterns between current-injection electrodes. The benefits in terms of improved EIT performance, however, were small for conditions in which the EIT measurements had been 'optimized' by the choice of stimulation and measurement patterns, as well as the algorithm and the use of fine EIT meshes.

Within the limited scope of this study, benefits from a tailored distribution were only observed for two cases. One case used a common EIT algorithm (One step Gauss-Newton reconstruction), for which a smooth tailored distribution with increased baseline conductivity in the center provided a better separation of two centrally located hot spots, as compared to a baseline uniform

conductivity. Another case used a TV (Total Variation) Reconstruction algorithm, and in this case the magnitudes of two hot spots near the center of the sensing skin were slightly better captured for a smooth tailored distribution with reduced conductivity in the center.

Overall, it can be concluded that EIT has strong potential for 2D temperature measurements. Future work should be devoted to the systematic determination of how the optimal combination of stimulation patterns, measurement patterns, and reconstruction algorithms change with the specific application. Such efforts should be prioritized over the use of tailored baseline distributions, which seem to provide relatively limited benefits.

DETAILED DESCRIPTION OF RESEARCH AND DEVELOPMENT AND METHODOLOGY:

This work was performed computationally in its entirety using the EIDORS package for EIT [3], executed in MATLAB R2022b. For convenience, the application examples shown here were developed based on the EIDORS tutorials published online by Adler [4]. Any referenced MATLAB scripts can be retrieved from either [3] or [4]. The EIDORS package includes algorithms for automated mesh generation, automated generation of different current stimulation patterns, automated generation of different electrode voltage measurement patterns, as well as multiple built-in reconstruction algorithms for solving the inverse problem.

New MATLAB code, however, had to be developed for the generation of tailored baseline conductivity (κ) distributions. This was done conveniently by tailoring the function calls to the build-in MATLAB script elem_select.m. Below is an example for the smooth baseline distribution with elevated conductivity in the center of a circular domain:

```
% Conductivity Modification Quadratic
scale_fcn = inline('(1.5-1*(x.^2+y.^2))','x','y','z');
img.elem_data = elem_select(img.fwd_model, scale_fcn);
```

The above distribution and others used in this study are shown graphically in Fig. 1. To superimpose ‘hot spots’ with locally reduced conductivity on these tailored distributions, a different function call of the built-in MATLAB script elem_select.m was performed.

```
% Add a hot spot with 50% conductivity, slightly above the center of the domain.
local_rel_cond_red = 0.50;
select_fcn = inline('(x-0.18).^2+(y-0.32).^2<0.1628^2','x','y','z');
img.elem_data_object = elem_select(img.fwd_model, select_fcn);
img.elem_data = img.elem_data - img.elem_data .* img.elem_data_object *
local_rel_cond_red;
```

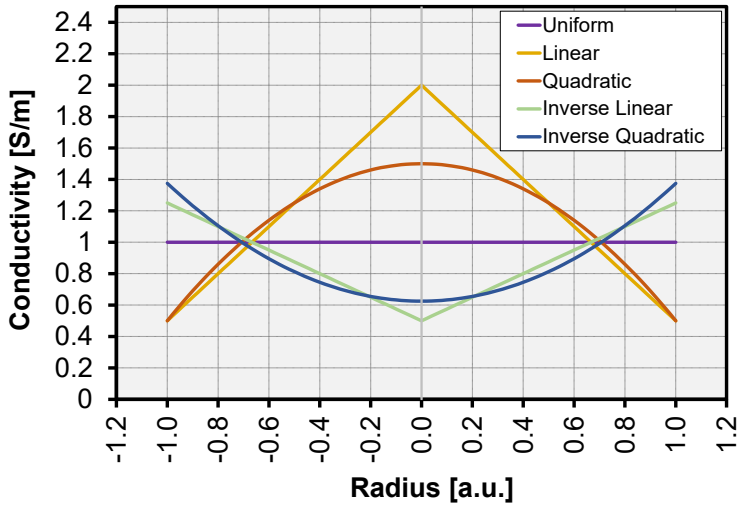

Figure 1 Conductivity vs. radius for the examined baseline distributions.

For an example with three hot spots with a local relative reduction of conductivity of 50% ($\Delta\kappa$ = -50%), this would then render conductivity distributions like those shown in Fig. 2.

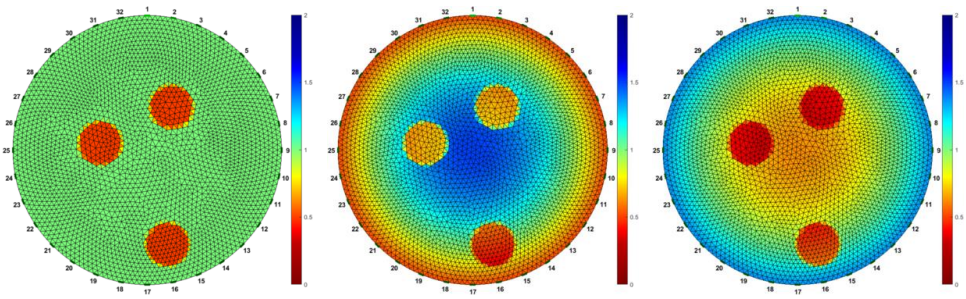

a) Uniform b) Quadratic c) Inverse Quadratic

Figure 2 Conductivity distributions with three hot spots with 50% local reduction in conductivity ($\Delta\kappa$ = -50%) for three different baseline distributions. Plotted scale = 0 – 2 for all three cases.

However, for most electrical conductors a change of local conductivity on the order of a few percent is a more realistic scenario [5]. Figure 3 shows such a scenario with $\Delta\kappa$ = -5% in the hot spots. In this case, the local change of conductivity in the hot spot is substantially lower than the total spread of baseline conductivity for the Quadratic and Inverse Quadratic cases.

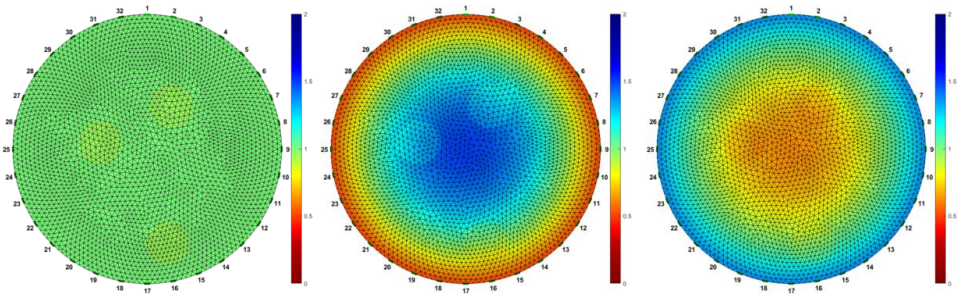

a) Uniform b) Quadratic c) Inverse Quadratic

Figure 3 Conductivity distributions with three hot spots with Δκ = -5% for three different baseline distributions. Plotted scale = 0 – 2 for all three cases.

EIT can be broadly categorized by the use of either absolute or difference methodologies, as discussed by Smyl [6]. Various numerical methods exist for image reconstruction in EIT. In absolute EIT, the conductivity distribution is reconstructed based on a single set of voltage measurements. Absolute EIT typically requires iterations to solve the nonlinear EIT problem. In difference EIT, the change in the conductivity between two states is reconstructed from voltage measurements that correspond to each of the two states. In this study, focus is given to the use of difference EIT since it provided better EIT performance. In addition, for temperature monitoring it can be argued that difference EIT is a natural choice since most applications are expected to facilitate reference measurements for which the 2D temperature field is uniform (*e.g.,* before system start-up). For the results presented below, relatively fine meshes were used for both the forward and inverse problems. The forward meshes shown in Figs. 2 and 3 were generated with the Netgen Mesher in EIDORS and have 2940 nodes, 5718 elements, and include 32 electrodes.

RESULTS AND DISCUSSION:

The combination of stimulation patterns and measurement patterns can influence the EIT performance greatly. As a starting point, the EIT performance is examined for the baseline uniform conductivity distribution and for three hot spots with a local reduction of conductivity of 5 % (Δκ = -5%). Five different reconstruction algorithms were used, following the EIDORS example by Adler in MATLAB script tutorial120a.m [7]. These five algorithms are listed in the caption of Fig. 4 and are used in the following figures.

The results show that the stimulation and measurement patterns and methodologies have a strong influence on the detection of hot spots with a 5% reduction of conductivity. By a visual comparison column by column in Fig. 4, the largest effects are found for algorithm 1) One step Gauss-Newton reconstruction (Tikhonov prior) and algorithm 3) One step Gauss-Newton reconstruction (Laplace filter prior), which both show great performance improvements for some

of the altered stimulation and measurement patterns. The nomenclature used here for the stimulation and measurement patterns reflects the definitions in the EIDORS package.

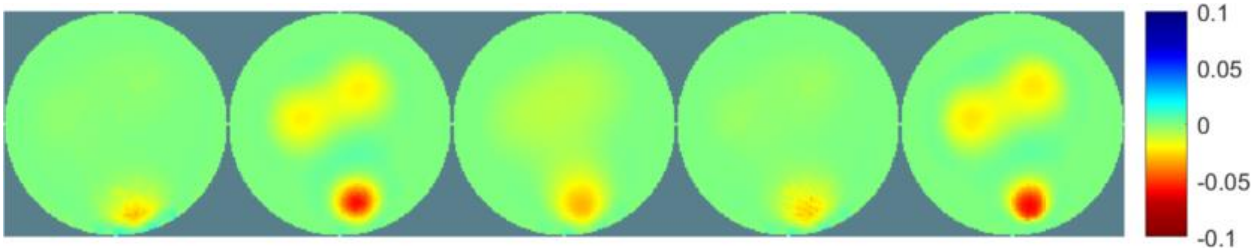

A: Adjacent Stimulation, Adjacent Measurement, No Measurement on Current-Injection Electrodes, Rotate Measurements, Without Noise.

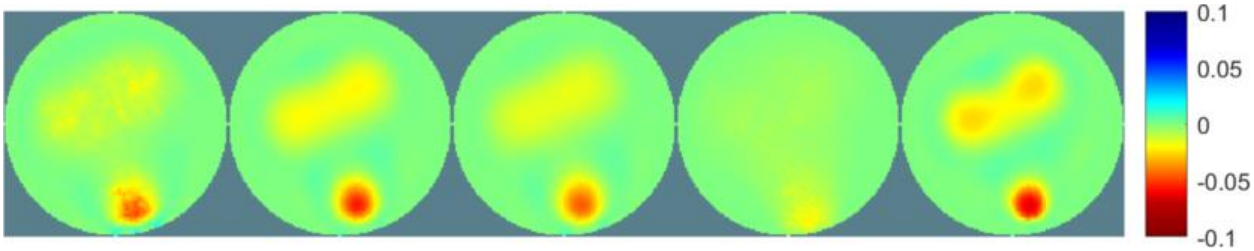

B: Opposite Stimulation, Adjacent Measurement, No Measurement on Current-Injection Electrodes, Rotate Measurements, Without Noise.

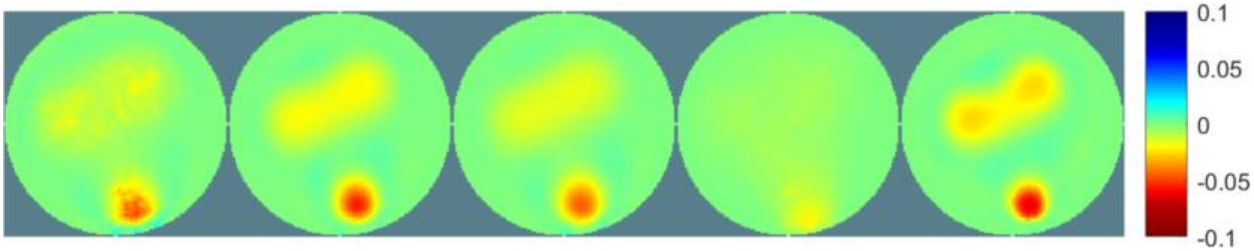

C: Adjacent Stimulation, Opposite Measurement, No Measurement on Current-Injection Electrodes, Rotate Measurements, Without Noise.

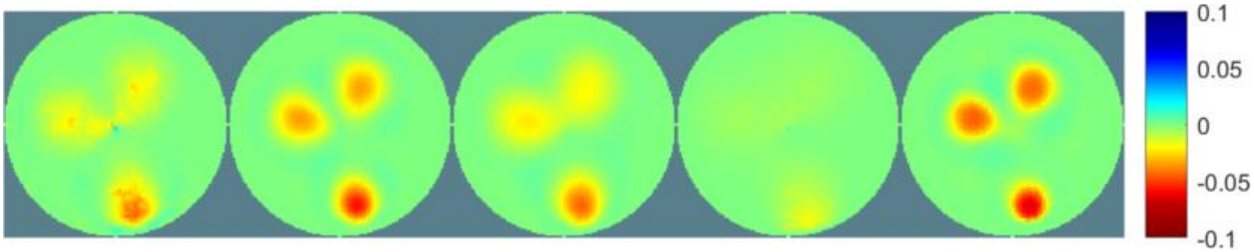

D: Mono Stimulation, Adjacent Measurement, Measurement on Current-Injection Electrodes, Rotate Measurements, Without Noise.

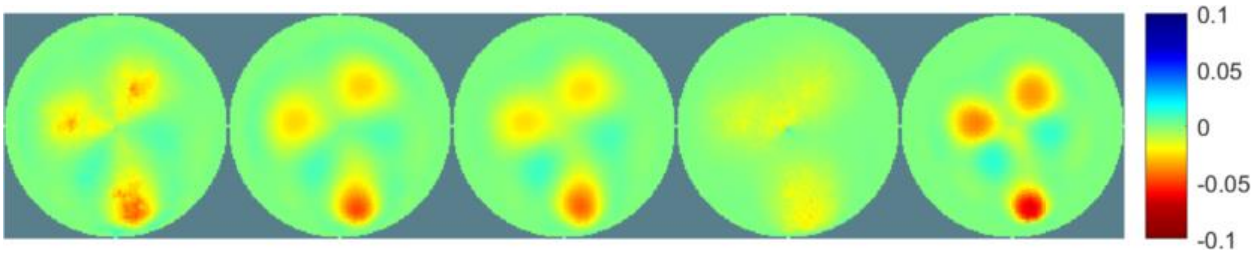

E: Mono Stimulation, Opposite Measurement, Measurement on Current-Injection Electrodes, Rotate Measurements, Without Noise.

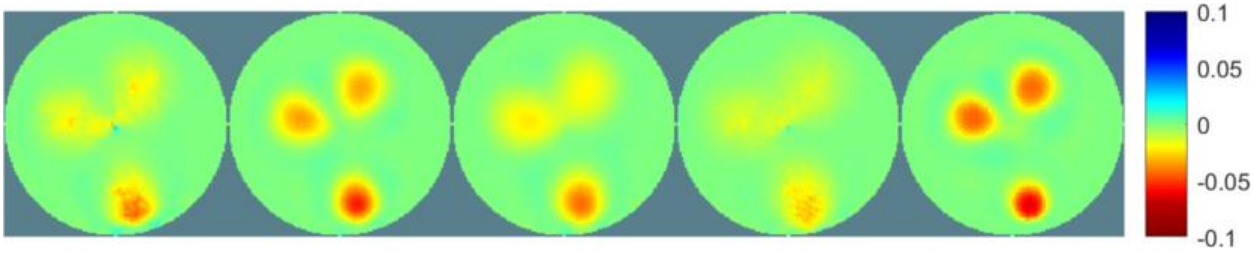

F: Adjacent Stimulation, Mono Measurement, No Measurement on Current-Injection Electrodes, Rotate Measurements, Without Noise.

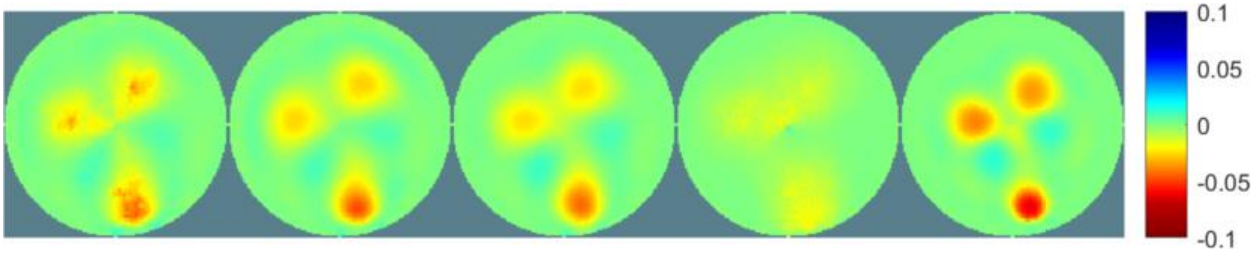

G: Opposite Stimulation, Mono Measurement, No Measurement on Current-Injection Electrodes, Rotate Measurements, Without Noise.

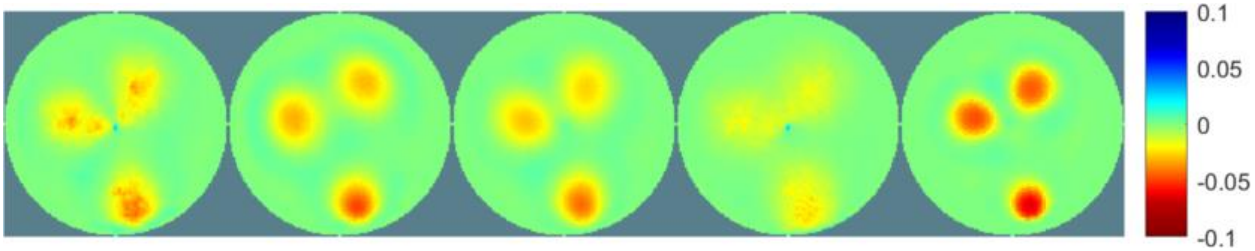

H: Mono Stimulation, Mono Measurement, Measurement on Current-Injection Electrodes, No Rotation of Measurements, Without Noise.

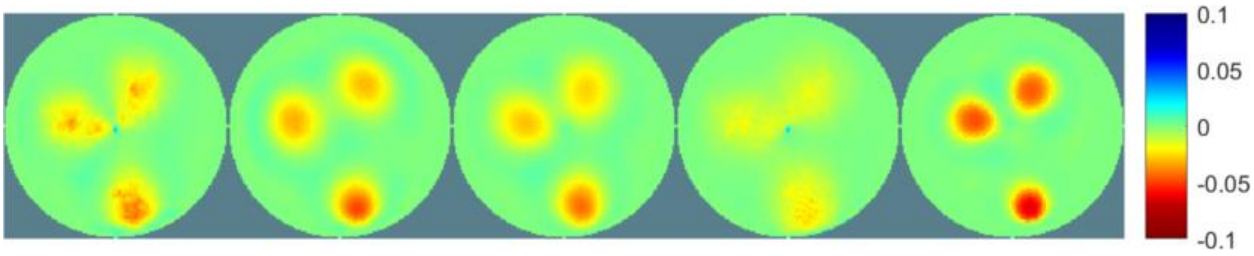

I: Mono Stimulation, Mono Measurement, Measurement on Current-Injection Electrodes, Rotate Measurements, Without Noise.

Figure 4 Effect of stimulation and measurement patterns (A-I) on the performance of five different reconstruction algorithms (from left to right): 1) One step Gauss-Newton reconstruction (Tikhonov prior), 2) One step Gauss-Newton reconstruction (NOSER prior), 3) One step Gauss-Newton reconstruction (Laplace filter prior), 4) One step Gauss-Newton reconstruction (with automatic hyperparameter selection), 5) Total Variation reconstruction. $\Delta\kappa$ = -5% and no simulation of measurement noise.

The top performing algorithms are 2) One step Gauss-Newton reconstruction (NOSER prior) and 5) Total Variation reconstruction. For these two, there are several stimulation and measurement patterns that provide near equally strong performance. The choice of stimulation and measurement patterns, however, must also consider susceptivity to noise. Hence, the simulations were modified to add measurement noise equivalent to a signal-to-noise ratio (SNR) of 48 dB and then repeated. The results are shown in Fig. 5.

The response to noise is overwhelming strong for cases H and I, indicating that those combinations of stimulations and measurement patterns are impractical. The effect of noise is also strong for case A. Hence, for further studies with hot-spot scenarios like this example, cases B, C, D, E, F, and G should be considered. Going forward, case F will be used since the performance is most even across the five algorithms.

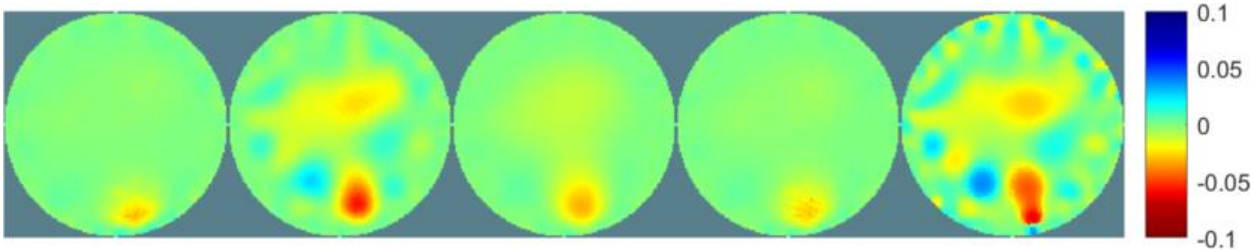

A: Adjacent Stimulation, Adjacent Measurement, No Measurement on Current-Injection Electrodes, Rotate Measurements, With Noise.

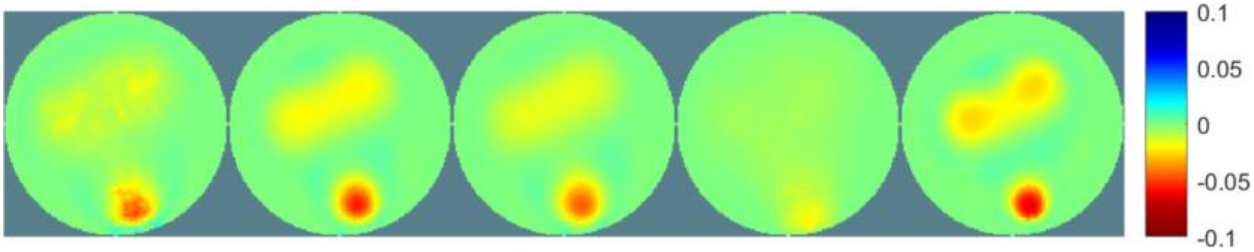

B: Opposite Stimulation, Adjacent Measurement, No Measurement on Current-Injection Electrodes, Rotate Measurements, With Noise.

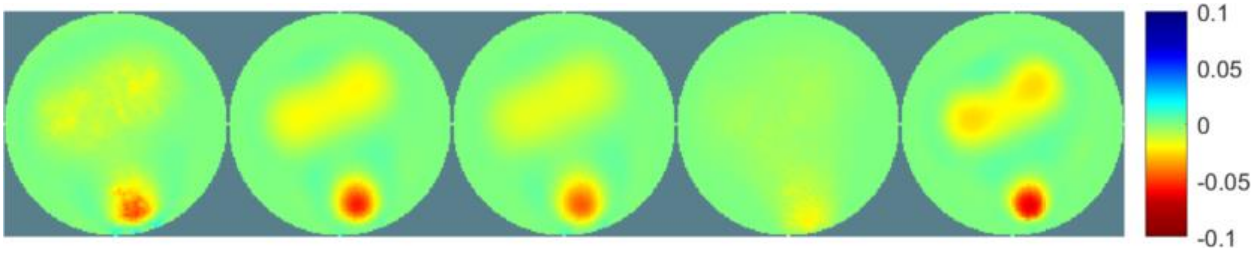

C: Adjacent Stimulation, Opposite Measurement, No Measurement on Current-Injection Electrodes, Rotate Measurements, With Noise.

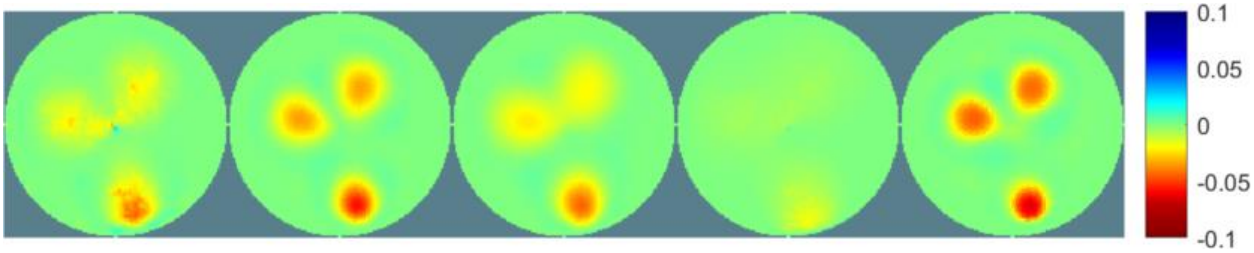

D: Mono Stimulation, Adjacent Measurement, Measurement on Current-Injection Electrodes, Rotate Measurements, With Noise.

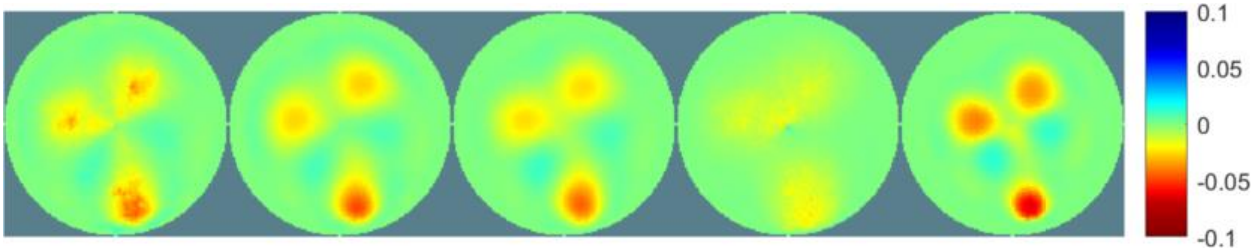

E: Mono Stimulation, Opposite Measurement, Measurement on Current-Injection Electrodes, Rotate Measurements, With Noise.

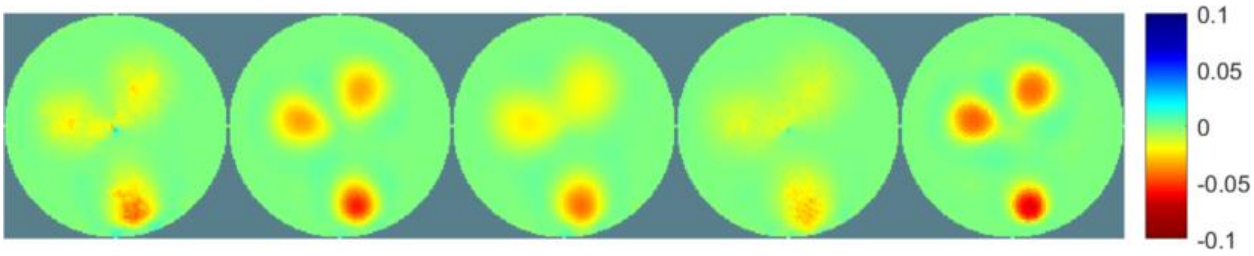

F: Adjacent Stimulation, Mono Measurement, No Measurement on Current-Injection Electrodes, Rotate Measurements, With Noise.

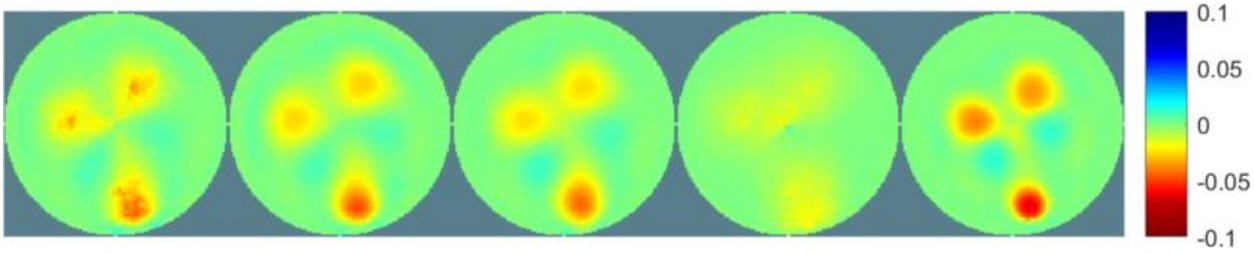

G: Opposite Stimulation, Mono Measurement, No Measurement on Current-Injection Electrodes, Rotate Measurements, With Noise.

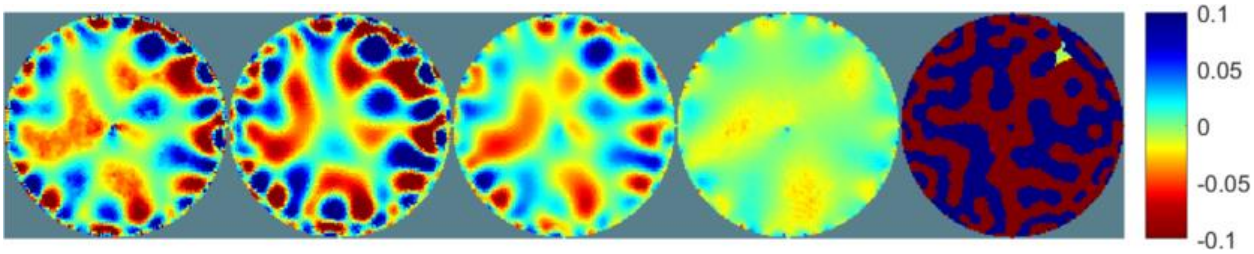

H: Mono Stimulation, Mono Measurement, Measurement on Current-Injection Electrodes, No Rotation of Measurements, With Noise.

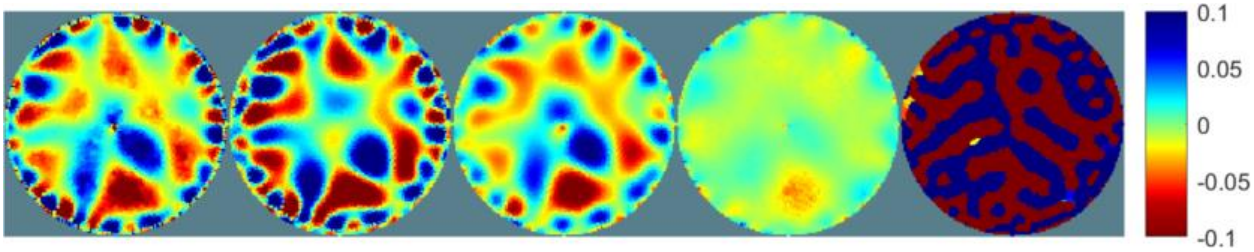

I: Mono Stimulation, Mono Measurement, Measurement on Current-Injection Electrodes, Rotate Measurements, With Noise.

Figure 5 Same as Fig. 4 but with random noise equivalent to a SNR of 48 dB added to the measured values. (Note, this is a simulation of noise since no actual experimental measurements were performed.) $\Delta\kappa$ = -5%.

In the following, case F will be used to evaluate how the EIT performance responds to changes of the baseline conductivity, as shown in Fig. 3. Again, we are evaluating three hot spots with a local reduction of conductivity of 5%, as shown for the three baseline distributions above.

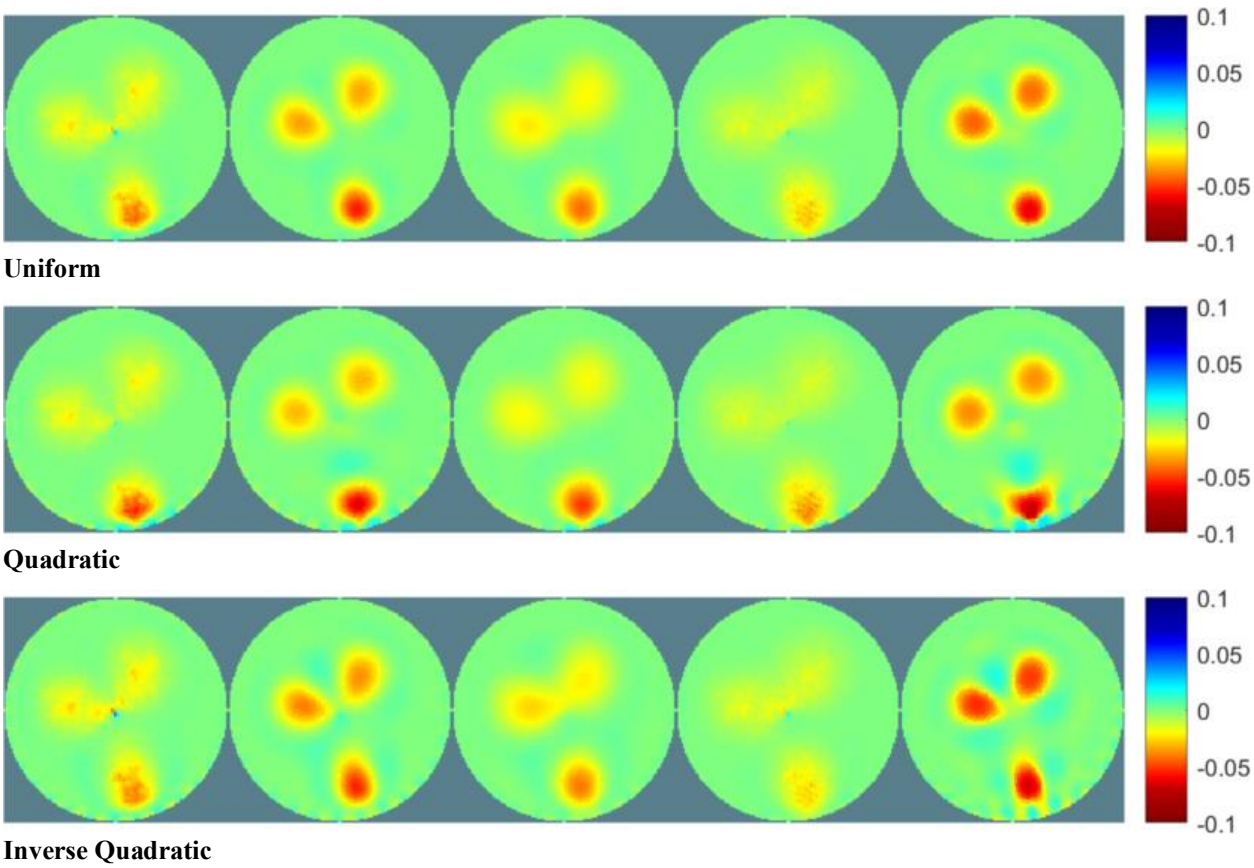

Figure 6 Effect of tailored baseline distributions for Case F with $\Delta\kappa$ = -5% and no simulation of measurement noise.

Without measurement noise, a change of the baseline distribution from uniform to either the Quadratic or Inverse Quadratic distribution does not provide much benefit for the two best performing algorithms 2 and 5. In fact, the non-uniform background distributions induce a moderate level of artifacts, especially for algorithm 5 (TV Reconstruction). The only small benefit of a tailored baseline distribution is seen for the Inverse Quadratic distribution for which the magnitudes of the two hot spots near the center are slightly better captured for algorithm 5. Figure 7 shows that these observations do not change with the addition of measurement noise since case F is relatively robust against noise.

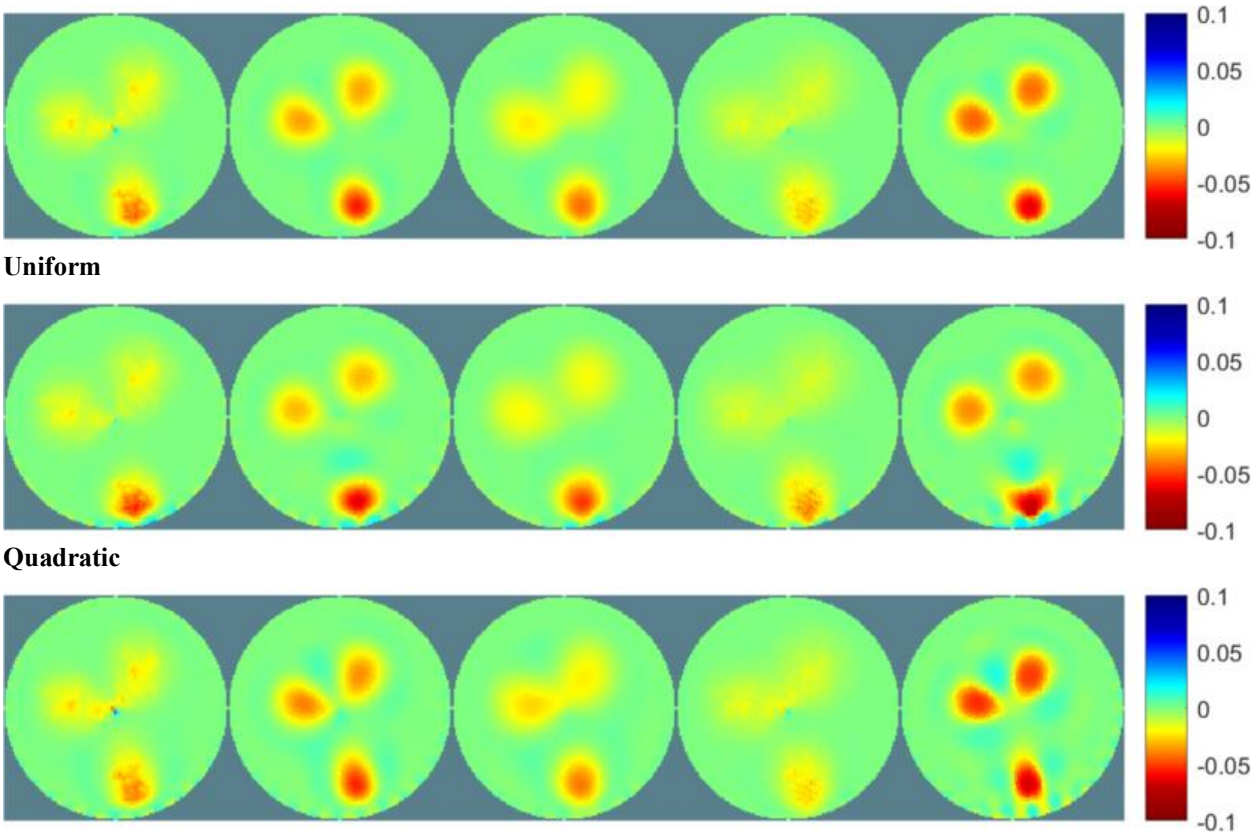

Figure 7 Effect of tailored baseline distributions for Case F with $\Delta\kappa$ = -5% and with simulation of random measurement noise equivalent to SNR = 48 dB.

Next, the three distributions were evaluated for a scenario with a much stronger reduction of the local conductivity $\Delta\kappa$ = -50%, as shown in Fig. 2. The results are plotted in Fig. 8. As discussed above, the stimulation and measurement pattern Case F was selected for its good performance with and without measurement noise for all five algorithms when the local reduction of conductivity was 5%. In this case with a much stronger reduction of $\Delta\kappa$ = -50%, it appears like the stimulation and measurement pattern Case F is no longer the best choice for all algorithms. In particular, algorithm 5 (TV reconstruction) shows artifacts along the lower edge. When the tailored baseline distributions were applied, the number of artifacts grew drastically for algorithm 5, especially for the Inverse Quadratic distribution. Under these conditions, the only real benefit from a tailored distribution was observed for algorithm 3 (One step Gauss-Newton reconstruction (Laplace filter prior)), for which the Quadratic distribution allowed a better separation of the two centrally located hot spots.

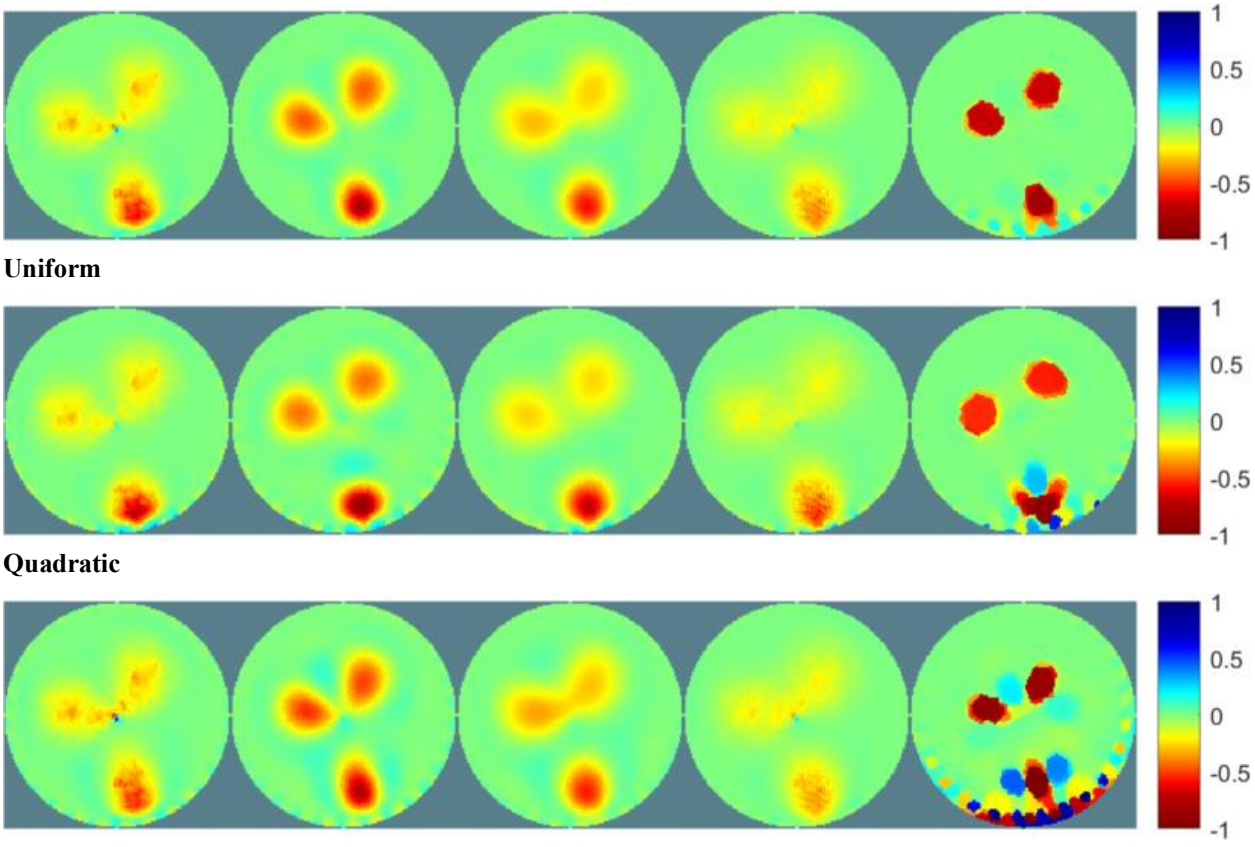

Figure 8 Effect of tailored baseline distributions for Case F with $\Delta\kappa$ = -50% and no simulation of measurement noise.

During the workflow of this study, many other combinations of mesh refinement, number of electrodes, stimulation and measurement patterns, and algorithms were examined. For some of the cruder models (which also require much shorter computational time) benefits of tailored baseline distributions were observed for certain combinations of hot spots. Hence, the use of the tailored distribution should not be discounted since it may provide sufficient benefits for specific circumstances. On the other hand, it may be challenging to generate 'sensing skin' for which the conductivity varies non-linearly with distance from the center. If that is the case, the use of linearly varying conductivity might be considered, as illustrated in Fig. 1. For the conditions of Figs. 6 & 7 with $\Delta\kappa$ = -5%, the difference between the EIT images for Linear and Quadratic was found be very small (not shown here). The same was true for the Inverse Linear and Inverse Quadratic distributions.

However, for some of the tested applications of absolute EIT, a substantial benefit of the smoother quadratic distribution was observed. Figure 9 shows an example for the Linear and Quadratic distributions.

Actual κ distribution

Reconstructed κ distribution

Actual Relative Value of κ

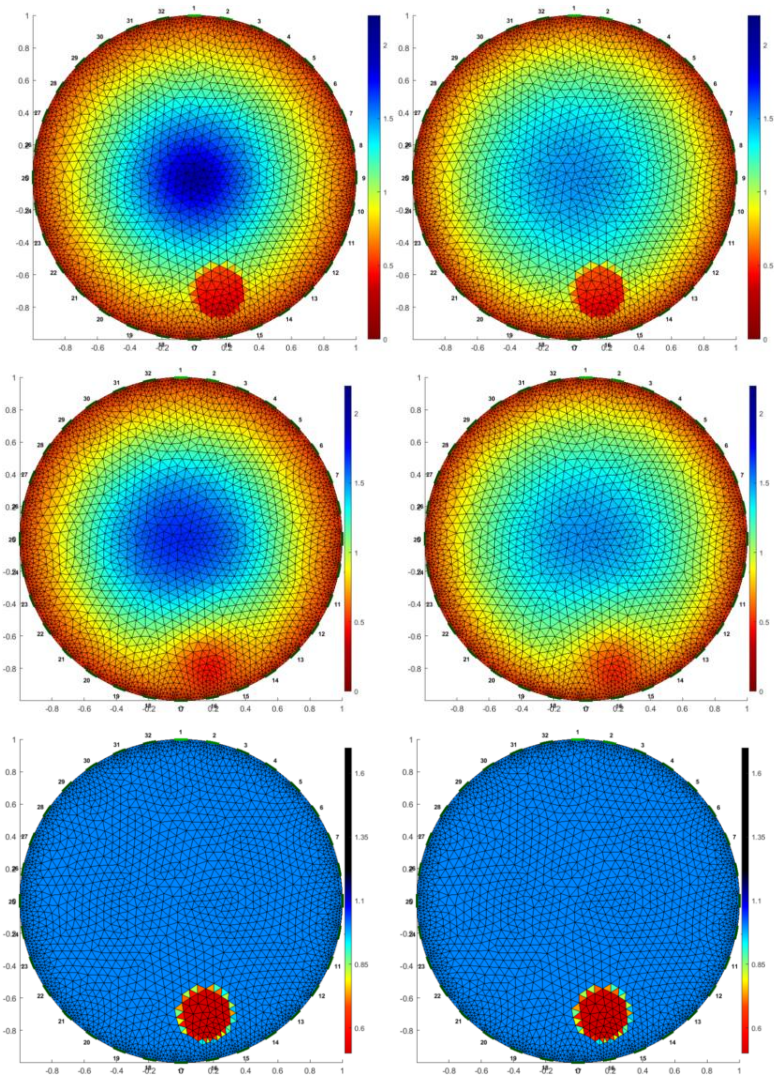

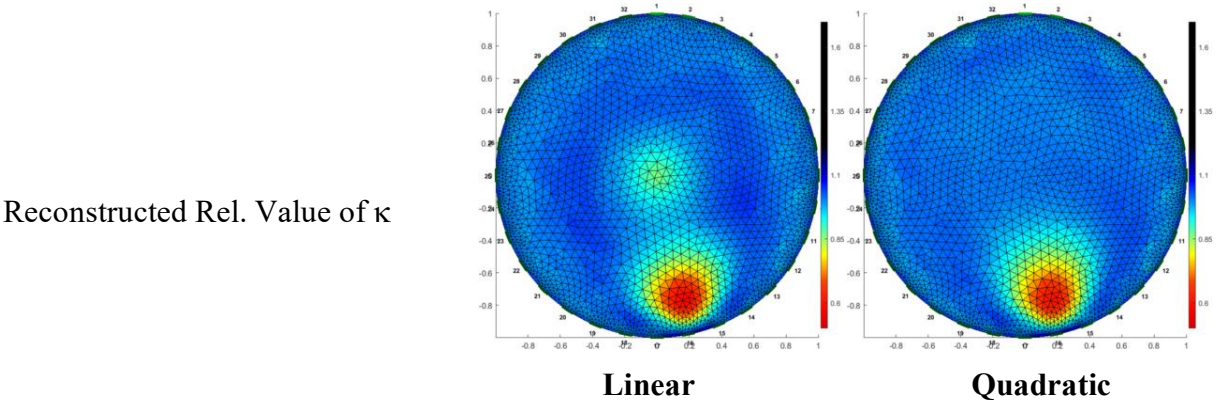

Figure 9 Comparison of Linear and Quadratic baseline distributions for Absolute EIT with Δκ = -50% and without simulation of measurement noise.

This example of absolute EIT followed the approach used to analyze tank phantom data acquired with 32 electrodes as contributed by Newell and explained by Adler [8]. This included the treatment of the electrode size and resistance. Figure 9 shows that the main difference is the strong reduction of artifacts for the Quadratic distribution, especially near the center. It can be noted from Fig. 1 that both linear distributions have conductivity gradients that change abruptly in the center of the domain, and this example of absolute EIT is clearly sensitive to such abrupt changes. Hence, for some EIT conditions, a smooth baseline conductivity distribution is preferred.

ANTICIPATED OUTCOMES AND IMPACTS:

Despite being a study of limited scope, the generated results clearly demonstrate that difference EIT has a strong potential to enable 2D-temperature measurements and hot-spot detection in settings in which brute-force thermocouple installation are impractical (*i.e.,* large-scale geometries). The original motivation for this study was to use tailored conductivity distributions to improve the accuracy of the EIT technique for hot-spot detection near the center of the 2D field, far away from the side-mounted electrodes. While it was demonstrated that tailored conductivity distributions can provide some benefits for specific scenarios, it also became clear that other factors are more important and should be given greater attention. These factors include the choice of inverse reconstruction algorithms. In the course of this work, various combinations of ‘standard’ choices for stimulation and measurement patterns and algorithms were examined. Hence, there are potentially substantial benefits that could be gained by developing and using new custom stimulation and measurement patterns, with the ‘optimal’ combination most likely dependent on the particular application and associated requirement for measurement accuracy.

It is suggested that future work should systematically quantify and document the effects of the numerous choices that are available for EIT temperature imaging, showing the trade-offs between experimental complexity, computational requirements, and measurement accuracy. Such knowledge is required for informed decisions of how to best implement temperature monitoring and hot-spot detection of large internal surfaces for which brute-force thermocouple installations are impractical.

It is anticipated that this SAND report will form the basis for a journal publication on this subject of EIT applications.

CONCLUSION:

It was found that the best approach for detecting a hot spot using EIT with a sensing skin depends on several factors. In particular, the magnitude of the relative reduction in local conductivity matters greatly, partly because it influences the choice of the most appropriate algorithm. For hot-spot detection using a sensing skin with a typical temperature coefficient of resistivity, the local reduction of the local conductivity may be limited to a few percent. Systematic studies of hot-spot detection with an assumed 5% reduction of local conductivity revealed that the ability to detect one or several hot spots was greatly influenced by three factors: 1. The current injection (stimulation) patterns, 2. The measurement patterns, and 3. The reconstruction algorithms. For a scenario with a 5% local reduction of conductivity, Case F was selected as the best choice of stimulation and measurements patterns (using Adjacent Stimulation, Mono Measurement, No Measurement on Current-Injection Electrodes, Rotate Measurements), providing good or reasonable EIT capability for five different algorithms evaluated here in a difference EIT framework: 1. One step Gauss-Newton reconstruction (Tikhonov prior), 2. One step Gauss-Newton reconstruction (NOSER prior), 3. One step Gauss-Newton reconstruction (Laplace filter prior), 4. One step Gauss-Newton reconstruction (automatic hyperparameter selection), and 5. Total Variation reconstruction.

In an effort to further improve the EIT capability, tailored baseline conductivities were assessed and compared to the baseline uniform conductivity. It was discovered that for some applications a tailored distribution needs to be smooth and that sudden changes in the conductivity gradients should be avoided. Two smooth distributions were assessed: one with higher baseline conductivity near the center of the measurement domain (named Quadratic), and another with reduced baseline conductivity near the center (named Inverse Quadratic). Simulations confirmed that the changes to the conductivity distribution had a substantial influence on the voltage distribution and the current-flow patterns between current-injection electrodes. Within the parameter space explored in this study, however, the benefits in terms of improved EIT performance were limited, especially for conditions in which the EIT measurements had been

'optimized' by the choice of stimulation and measurement patterns, as well as the choice of algorithm and the use of fine EIT forward and inverse meshes.

The EIT parameter space is very large, making a comprehensive assessment of the benefit of tailored baseline distributions challenging. Within the limited scope of this study, benefits from a tailored distribution were only observed for two scenarios: 1. Using reconstruction algorithm 3 (One step Gauss-Newton reconstruction (Laplace filter prior)), for which the Quadratic distribution was discovered to provide a better separation of two centrally located hot spots, as compared to a baseline uniform conductivity. 2. Using algorithm 5 (TV Reconstruction), for which magnitudes of the two hot spots near the center were slightly better captured for the Inverse Quadratic distribution.

REFERENCES:

1. J. Hewson *et al.*, "Predicting and Mitigating Cascading Failure in Stacks of Lithium-Ion Cells", SAND2019-11411C
2. R. Rashetnia, M. Hallaji, D. Smyl, A. Seppänen and M. Pour-Ghaz, "Detection and localization of changes in twodimensional temperature distributions by electrical resistance tomography", Smart Mater. Struct. 26 (2017) 115021, https://doi.org/10.1088/1361-665X/aa8f75
3. EIDORS 3.10 with Netgen 5.3, released 31 December 2019, http://prdownloads.sf.net/eidors3d/eidors-v3.10-ng.zip
4. EIDORS tutorials, http://eidors3d.sourceforge.net/tutorial/tutorial.shtml
5. Nichrome Alloys for Heating Applications, https://super-metals.com/wp-content/uploads/2015/04/Nichrome-Alloys-for-Heating.pdf
6. D.J. Smyl, "Electrical Imaging and Numerical Simulation of Unsaturated Moisture Flow in Cement-Based Materials", Ph.D. thesis North Carolina State University, 2017.
7. A. Adler, EIDORS tutorial "Compare 2D image reconstructions", 2012 http://eidors3d.sourceforge.net/tutorial/EIDORS_basics/tutorial120.shtml
8. http://eidors3d.sourceforge.net/tutorial/EIDORS_basics/rpi_data.shtml